Functional behaviour and microscopic analysis of ammonium sensors subject to fouling in activated sludge processes

Functional behavior and microscopic analysis of ammonium sensors subject to fouling in activated sludge processes

WATER IMPACT STATEMENT

We studied the evolution with time of fouling and functionality of ammonium sensors in wastewater. Microscopy and spectroscopy provided mapping of the surface morphology and the elemental composition of inorganic precipitates (in order of prevalence: Fe, P, Ca, Mn, S, K, and Cl). The drift of the fouled sensor is directional and downwards, indicating that with time the sensor underestimates real concentrations. Also, step-change experiments confirmed the increase in sensor response time.

Functional behaviour and microscopic analysis of ammonium sensors subject to fouling in activated sludge processes

Francesca Cecconi[1], Samuel Reifsnyder[1], Reza Sobhani[2,3], Albert Cisquella-Serra[4], Marc Madou[4], Diego Rosso[1,2, *]

[1]*Department of Civil and Environmental Engineering, University of California, Irvine, CA 92697-2175 (USA)*

[2]*Water-Energy Nexus Center, University of California, Irvine, CA 92697-2175 (USA)*

[3]*Orange County Sanitation District, 10844 Ellis Ave, Fountain Valley, CA 92708*

[4]*Department of Mechanical and Aerospace Engineering, University of California, Irvine, CA 92697-3975 (USA)*

[*]*Corresponding author (e-mail: bidui@uci.edu)*

Abstract – Fouling is an issue associated with all sensor instrumentation deployed in wastewater that causes a loss in sensitivity and reproducibility of the sensor elements, thus requiring frequent re-calibration. This paper presents a comprehensive analysis of the fouling development in activated sludge process with a case study on ammonium sensors and Ion-Selective Electrodes technology. The response time of the electrodes is found to be the most impacted by fouling. By analysing step-change experiments with a diffusion model, after one week of fouling the response time is demonstrated to increase exponentially with time. The performance of the sensor is also affected in terms of measurement accuracy, showing a negative drift of the fouled sensor (-0.11 mg NH_4^+ $l^{-1}d^{-1}$). Scanning electron microscope analysis and energy dispersive x-ray spectroscopy elemental mapping were performed over new and used sensor membranes to study the irreversible fouling composition and morphology. Fouling appears as thick coating with different agglomerates and crevasses, which reveal damages on the PTFE protective layer of the membrane. Fe, P, Ca, Mn, S, K and Cl were the main elements detected, in decreasing order. The high content of Fe in the fouling layer originates from the addition of ferric salts to the primary treatment of the plant, which becomes a major contributor to the inorganic fouling of the sensor. The study also quantifies the increase in Total Suspended Solids (TSS), Volatile Suspended Solids (VSS), and total Fe in the reversible fouling layer over time as described by a saturation model. However, the relative composition remains stable: 84% of VSS/TSS and 20% of Fe/iSS, on average.

Key Words - Ammonium, drift, electron microscopy, fouling, ion-selective electrode, online sensors.

33   **INTRODUCTION**

34   In recent years, many water resources recovery facilities (WRRFs) focusing on water reclamation

35   have faced stricter limits for nutrients discharge.[1,2] Continuous online measurements are

36   fundamental to deploy new and improved control strategies, which would otherwise not be

37   possible with a low sampling frequency rate. In addition, the increasing trend towards water reuse

38   has led to the high frequency monitoring of effluent quality to guarantee the safety of reclaimed

39   water.[3] Among the different water quality constituents, recent focus has been given towards online

40   ammonium quantification for both monitoring and control purposes. The ability to obtain

41   continuous ammonium measurements has allowed the implementation of ammonium-based

42   aeration control to optimize the air delivery of the aeration system with consequent reductions in

43   energy use.[4,5,6] Recently, ion-selective electrode (ISE) sensors have largely being deployed for

44   online ammonium measurement due to their fast response, low initial capital investment and

45   absence of analytes consumption and filtration unit requirements. In detail, ammonium ion-

46   selective electrodes are constituted by a polymeric membrane, often PVC $(C_2H_3Cl)_n$ plus

47   plasticizer, that contains a specific ionophore for the target analyte. However, the polymeric

48   membrane can easily be damaged by exposure to harsh environments and is characterized by low

49   durability. Usually, the membrane is also coated with a layer of PTFE $(C_2F_4)_n$, which provides a

50   hydrophobic surface, as a result of the low surface energy and surface roughness of the material,

51   that reduces and delays the adhesion of bacteria on the membrane.[7,8,9]

52

53   *Fouling of sensors*

54   Fouling is an issue associated with all sensor instrumentation that is deployed in water/wastewater

55   environment, which causes a loss in sensitivity, reproducibility and necessitates frequent re-

56   calibration requirements.[10,11] In addition, fouling decreases the operating lifetime of the sensor and

57   introduces a degree of error in the collected data.[10,12] This is because as fouling develops, an

58   artificial environment around the sensing surface is established, therefore the measured data will

59   not be truly representative of the location sampled.[13]

60

61   *Analogy with membrane filtration fouling*

62   A limited amount of studies has examined the fouling coating composition and the quantitative

63   impact of fouling on sensors performance. On the other hand, fouling development on filtration

64   membranes (both microfiltration and ultrafiltration) and its effect on the filtration performance has

65   been a widely investigated topic.[14,15,16,17] Given the similarity in the membrane composition

66   (polymers), and the analogy in the application (long-term operation in wastewater), literature

67   studies regarding the fouling of filtration membranes can provide a useful comparative reference

68   when approaching the fouling of ISE sensors.

69   Among the factors influencing the fouling development on filtration membranes, the iron content

70   in wastewater was shown to increase the fouling rate due to the rapid formation of colloidal iron

71   oxides.[18] Coagulants such as ferric chloride and aluminum sulfate are commonly used in water and

72   wastewater treatment for chemical precipitation, including phosphorous removal, and/or for odour

73   control purposes.[19,20,21,22,23,24,25] Iron dosage in wastewater can lead to severe filtration membrane

74   fouling due to the formation of both amorphous ferric oxyhydroxide particles and gelatinous

75   aggregates containing Fe(III), which bind to polysaccharide materials, and are responsible

76   especially for irreversible membrane fouling.

77   In consideration of the scarcity of literature on sensor fouling in wastewater treatment, the goal of

78   this paper is to provide a detailed analysis of the fouling development with a case study on

79   ammonium sensors. To achieve this goal, we studied two parallel ISE-NH$_4^+$ sensors, installed in

80   the aeration tank of an activated sludge process. The effect of fouling on the sensor performance

81   was investigated by analysing sensor response time, signal drifting and operating lifetime of the

82   electrodes. Moreover, the fouling morphology and composition was examined using scanning

83   electron microscopy (SEM) and energy dispersive x-ray spectroscopy (EDX), respectively.

84   **MATERIALS AND METHODS**

85   A set of two ISE-ammonium sensors (Horiba model HC-200NH) were installed in the aeration

86   zone of a WRRF's secondary tank. The facility is located in the Southwestern United States,

87   characterized by an arid to semi-arid climate. The secondary treatment of the plant includes an

88   activated sludge process operating in the Ludzack-Ettinger configuration, divided into six zones

89   in series, with an annual average SRT of 5 days and Mixed Liquor Suspended Solids (MLSS) of

90   2700 mg L^{-1}. The process is operated in step-feed mode, with a 60/40 split between the first and

91   third zones, which are operated under anoxic conditions. The temperature of the wastewater in the

92   aeration tank ranges from 25°C to 30°C, between the winter and summer season, respectively. A

93   rack composed of ten ammonium ion-selective-electrodes was built and immersed in the activated

94   sludge tank, next to the sensors previously mentioned (See Appendix, Fig. A.1). The rack was used

95   to study the reversible fouling development and composition on the electrodes' surface over time.

96   Further information on the governing principles of ISE sensors can be found in the Appendix (ISE

97   technology description). Also, an extended report of the following Materials and Methods is

98   presented in the Appendix.

99

100   *Step-change experiments*

101   The response time of the ammonium sensor was measured by performing step-change experiments

102   according to the ISO 15839[26] as described in Rieger et al. (2003).[27] Specifically, the step-change

103   experiments were performed switching between two standard solutions of 10 mg L^{-1} and 25 mg L^{-}

104   ^{1} of ammonium. First, the sensor was subject to an abrupt change from the lower solution to the

105   higher. Following the stabilization at the higher concentration, the sensor was switched back to the

106   lower concentration solution. The response time of the ISE sensor can be described by a diffusion

107　　process. Similarly to Morf et al 1975[28] and Frankær et al 2019[29], an exponential diffusion model

108　　was formulated to calculate the volumetric mass transfer coefficient, k, for both the rise and fall

109　　times of the step-change experiment (see Appendix, Step-change experiment).

110

111　　*Iron measurements*

112　　Ferric chloride is continuously added in the primary clarifier of the treatment plant to ensure a

113　　concentration of 24 mg L^{-1} for odor control. Therefore, total iron measurements were performed

114　　on both grab samples of wastewater and for the fouling accumulated on the ISE membranes, in

115　　order to investigate the contribution of iron on the fouling development. The iron content analysis

116　　was performed both on the fouling accumulated over the sensor and over the rack electrodes, using

117　　the same procedure.

118

119　　*SEM – EDS*

120　　The membrane surfaces of the ammonium electrodes were analyzed in pristine conditions and after

121　　six months of activity in the aeration tank. FEI MAGELLAN 400 XHR scanning electron

122　　microscope was used to obtain SEM images of the membranes, to visualize the effect of

123　　irreversible fouling at a micron scale and compare the changes in membrane morphology with

124　　time. Additionally, complementary EDX elemental mapping of different areas of the membranes

125　　were obtained in new and used membranes to identify the main fouling elements.

126   **RESULTS AND DISCUSSION**

127   The sensor performance was evaluated under different degrees of fouling development, depending

128   on the cleaning frequency adopted. As previously mentioned by Cecconi et al., 2019,[30] two types

129   of fouling were recognized (See Appendix, Fig. A.2.): reversible fouling, building up as a thick

130   layer and dependent on the cleaning frequency; and irreversible fouling, developing over long-

131   term operations, which cannot be removed via normal cleaning procedures.

132

133   *Response time*

134   Figure 1 shows a graphical explanation of the transport phenomena of ammonium from the bulk

135   of the solution to the electrode's membrane interface under cleaned and fouled conditions.

136   The transport process of a clean ISE membrane can be represented by its equivalent electrical

137   circuit (Fig. 1.a).   In detail, the impedance spectrum, which describes the electrochemical

138   behaviour of the sensor, is composed of four circuit elements: R_B (bulk resistance), C_{dl} (double

139   layer capacitance), R_{ct} (charge transfer resistance), and W_E (Warburg impedance).[31,32,33] The

140   fouling development adds an additional diffusional resistance layer which characteristics could be

141   further analysed by impedance spectroscopy (Fig. 1.b).[34] Therefore, depending on the level of

142   fouling, the sensor's response to concentration fluctuations in the bulk solution is expected to show

143   a delay.

144

145

146

147   To demonstrate the effect of fouling on sensor performance, the response time of the sensor was

148   measured at different fouling conditions by performing step-change experiments.

149   Figure 2.a shows the example of a step-change experiments performed under cleaned conditions.

150   An example of the step-change experiment conducted on a fouled membrane can be seen in the

151   Appendix, Fig. A.3. The results are reported in mV and the sensor's signal was recorded every 5

152   seconds. The diffusion model was fitted to the signal for every experiment during the rise and fall

153   time at different fouling conditions and presents, on average, a coefficient of determination R^2 of

154   0.95. For each test conducted, the volumetric mass transfer coefficient (k) was calculated both for

155   the rise and the fall times (see Appendix, Table T.1). The mass transfer coefficients calculated for

156   each fouling condition (averaging between the rise and the fall time) are reported in Fig. 2.b as

157   function of the time of fouling development.

158

159

160   After a lag-time of approximately one week, where no evident effect on response time was noticed,

161   the volumetric mass transfer coefficient showed an exponential decrease with the time of fouling.

162   Thus, under these specific process conditions, a cleaning frequency of more than once per week

163   was not required. The exponential decay model, reported in Fig. 2.b, presents a coefficient of

164   determination R^2 of 0.97. Therefore, it highlights how the fouling development in time on the

165   sensor membrane results in the exponential increase of the response time of the sensor. This impact

166   on the sensor responsiveness can indeed pose a limit on its capacity to follow the dynamics of the

167   ammonium content in the wastewater. The experiments performed after protracted periods of

168   fouling (3 or 4 months), show small differences in response time between before and after cleaning.

169   Thus, as the sensor's electrodes gradually begin to approach the end of their operating lifetime,

170   the irreversible fouling becomes the main contributor in increasing the response time of the sensor,

171   regardless of the cleaning frequency. Therefore, for short-term operating periods (2 to 4 weeks),

172   the reversible fouling is the main factor influencing the sensor performance, whereas, for the long-

173   term operating periods (3 to 5 months), the irreversible fouling is the main contributor behind the

174   increase in sensor response time. Due to the challenges associated with the prevention of the

175   irreversible fouling development, the response time of the sensor is inevitably expected to increase

176   during the lifetime of the electrodes, which therefore can be considered one of the main factors

177   associated with the "aging" of the electrodes.

178

179   *Drift behaviour*

180   If not periodically recalibrated, every sensor is subjected to drift phenomena in the long term, even

181   if regularly cleaned.[35,36] Drift, expressed as a loss of sensitivity, occurs even when well maintained,

182   and is typically caused by physical changes in the sensor and/or by environmental contamination.

183   Therefore, the drift behaviour of a well-maintained ammonium sensor during its whole lifetime

184   was analysed by comparing the reading of the sensor with lab analysis on grab-samples. During

185   the study, the sensor was manually cleaned twice a week, no other maintenance and operation

186   procedures were conducted, and no changing in process operation or in the wastewater

187   composition was recorded. Further details on the maintenance and operation procedure of the

188   sensors can be found in the Supplementary Information (Technology validation procedure and

189   maintenance). On average, the comparison with lab analysis was conducted every 3 days,

190   collecting 5 samples over a 3 hours span. Figure 3 shows the comparison between the lab

191   measurement and the sensor reading during 4 months of operation. The dataset is divided into

192   months, from the first month after the calibration of the sensor (red triangles) till the fourth month

193   (blue diamonds). The intercept and slope of the first month was normalized to 0 and 1, respectively.

194   The data of the other months (from 2 to 4) were normalized relatively to the first month dataset.

195

196

197

198   From Fig. 3 it is evident that the sensor incurs drift over time with a negative trend of -0.01 mg

199   NH_4^+ l^{-1} d^{-1}, which leads to an inexorable underestimation of the ammonium content in wastewater.

200   Despite that reversible fouling development is prevented by adopting a consistent cleaning

201   procedure, the ammonium sensor still requires a recalibration every 3 months, which corresponds

202   to a loss of accuracy of ~1 mg l^{-1} of ammonium. Subsequently, the performance of the ammonium

203   sensor, in terms of signal accuracy, was evaluated under fouling development. The differences

204   between the signals of two parallel ammonium sensors were analysed over time. One sensor was

205   not cleaned for 20 days while the other sensor, installed in the same tank right next to the other

206   sensor, was cleaned twice a week in order to prevent the fouling build-up. The same experiment

207   was conducted three times for 20 days each. Figure 4 shows in blue the difference between the two

208   sensors (expressed as cleaned sensor signal minus the fouled sensor signal) at a 2-minute

209   frequency. The top right insert shows the comparison of the drift trend of the cleaned sensor

210   previously measured (in orange) with the drift trend measured with the current fouling experiment

211   (in blue).

212

213   The fouling leads to an underestimation of the ammonium reading, which degrades in time with a

214   monotonically decreasing trend. The drift, calculated from the three experiments, presents a slope

215   of -0.11 ± 0.03 mg NH_4^+ $l^{-1}d^{-1}$. The slope of the linear trend of the fouled sensor is one order of

216   magnitude higher (-0.11 mg NH_4^+ $l^{-1}d^{-1}$) than the drift of the cleaned sensor (-0.01 mg NH_4^+ $l^{-1}d^{-1}$

217    $^{-1}$), showing that a fouled sensor drifts much faster than a cleaned one. These results highlight the

218   importance of adopting a consistent maintenance procedure, since it was demonstrated that fouling

219   also affects the absolute accuracy of the sensor reading, independently on the response time of it.

220   The position of the sensor installation along the aeration tank can also influence the sensor fouling

221   since the wastewater composition changes along the process. Therefore, it can be expected a faster

222   fouling development for an influent installation, and therefore a larger drift slope if the sensor is

223   left unmaintained compared to the same type of sensor installed in the effluent.

224

225

226   *Iron analysis*

227   Analysis of the iron content, due to the addition of ferric salts in the primary treatment at the

228   facility, was conducted on the reversible fouling layer. The iron composition of the fouling layer

229   was investigated over time. Fouling was collected from the electrode membranes of both the two

230   sensors and from the rack immersed in the wastewater, containing 10 electrodes (See Appendix,

231   Fig. A.1). A summary of the fouling and wastewater composition over time, in terms of total iron,

232   VSS, and TSS is reported in the Appendix, Table T.2.

233   After a preliminary examination, it was observed that the iron present in both wastewater and

234   fouling was mainly in the form of Fe(III) and was absorbed to the solids' surface since no trace of

235   iron was detected on filtered samples. This result is in accordance with the findings of Kazadi

236   Mbamba et al (2019)[37] and Wang and Waite (2010)[38], regarding the iron speciation in wastewater.

237   Figure 5a shows the trend of TSS, VSS and total iron collected from the surface of the rack's

238   electrodes during the period of fouling development. The data was analysed with a saturation

239   model, for TSS, VSS and iron accumulation, showing a R^2 of 0.95, on average. In time, solids

240   accumulate on the surface of the electrode, creating a thick layer of fouling. After one month, the

241   growth of fouling decreases eventually reaching a balance between fouling accumulation and

242   detachment, due to the shear stress provoked by the aeration bubbles and the wastewater flow. At

243   seven weeks of fouling a foaming event of the treatment plant had influenced the fouling

244   composition, which was then treated as an outlier. Due to the excess of foam, the rack was covered

245   in bubbles, which had dispersed the fouling layer that had developed previously. The same

246   increasing trend of fouling build-up was noticed also on the analysis performed on the fouling

247   samples collected from the sensor's surface (see Appendix, Fig. A.4), which shows a similar

248   behaviour with the results obtained for the rack's electrodes experiments. Figure 5b presents the

249   ratio of VSS/TSS and Fe/iSS of the fouling composition over the time of fouling development,

250   comprising fouling samples collected from both the rack's electrodes and the sensor's surface.

251   Even if the accumulation of iron and solids on the surface increases over time, the relative

252   composition is relatively stable: 84% of VSS/TSS and 20% of Fe/iSS, on average.

253

254

255

256

257   Furthermore, after the 6 months in operation, the electrode membranes were cleaned with water

258   and were detached from the electrodes. TSS, VSS, and iron analyses were conducted on the

259   membranes of four electrodes, using the same methodology adopted for the reversible fouling

260   analysis. On average, the membrane was composed of 48 ± 10 µg of Fe, which represents the 2%

261   of the total membrane composition and 17% of the inorganic compounds content. The

262   accumulation of iron salts was then observed both on the reversible fouling layer and attached to

263   the membrane, in the irreversible fouling. Finally, the addition of FeCl as coagulant in the primary

264   clarifier is a very common practice and the composition analysis for this study points out that the

265   presence of high concentration of iron in the wastewater largely influences the inorganic fouling

266   development. It can be inferred that other plants that utilize the same coagulants application could

267   find similar issues with the development of inorganic fouling.

268

269

270   *Scanning Electron Microscopy*

271   Scanning Electron Microscopy was used to characterize the morphology and composition of the

272   irreversible fouling, which plays an important role on the aging of the electrodes as well as on the

273   performance of the sensor itself. Fig 6 shows surface sections of new and used electrodes'

274   membranes analysed with SEM. The used membranes were collected after six months of operation

275   of the sensor in wastewater, at the end of the lifetime of the electrode.

276

277

278   The clean membrane shows a homogeneous surface and the porous structure of the membrane is

279   clearly visible in the magnified image (Fig. 6.a). The used membrane (Fig 6.b) instead shows a

280   rough surface, with different type of agglomerates, crevasses and the pores of the original

281   membrane are not visible anymore, completely covered by the coating of the fouling which appears

282   dense and non-porous. The fouling SEM pictures of the sensor membranes show similarities

283   mainly with organic fouling of filtration membranes,[39] since evidence of specific precipitate

284   structures and scaling are scarce, and no microbial colonies can be observed. Different areas of the

285   fouled membranes' surface were analysed at different levels of magnification to recognize

286   different agglomerates and details (See Appendix, Fig. A.5 and A.6). Analogously to the observed

287   SEM pictures of fouling on microfiltration membranes, the fouling on the sensor develops as a

288   cake or gel layer, composed of bacteria clusters and biopolymers, which is indicator of biofouling

289   formation.[40,41,42]

290   The cracks and crevasses in the fouling, highlighted in Fig. 6.b, are numerous, dense and get

291   extended for large portions of the fouled surface. Such cracks, which are fibrous in nature, denote

292   a typical behaviour of polymers under stress, and originate from the stretching and damaging of

293   the PTFE protection layer. Also, the crevasses show a clear similarity to other SEM pictures of

294   stretched PTFE membranes obtained under stress reported in literature, which are characterized

295   by the same type of fibre-like stretch typical of polymers.[43,44] The same type of sample preparation

296   to perform SEM and EDX analysis, which procedure is described in the Appendix, was employed

297   on both the fouled and the new membranes. The PTFE cracks were never detected in new

298   membranes, which instead always showed a homogenous surface (see Appendix Figure A.7), and

299   therefore it can inferred that the PTFE protective layer damages originated during the six months

300   of activity of the sensor in wastewater, and not from the handling of the sensor membranes during

301   the SEM experimental procedures.

302   EDX elemental analysis was applied to the clean and fouled membranes for each of the previous

303   sections analysed with SEM. Quantitative analysis in EDX is only used as an estimation due to the

304   error of quantification of light elements such as oxygen, nitrogen and carbon but is useful for

305   polymer materials that have unique elemental signatures such as the fluorine of PTFE.

306   Furthermore, the atomic percent distribution obtained helps to estimate the relative proportion of

307   some contaminants like salts and metal oxides. A summary of the quantitative analysis of the

308   elements for each of the sections mapped with EDX technique on the new and used membranes

309   and the statistical error are reported in the Appendix, Table A.3. By comparing the difference in

310   composition between new and used membrane, it is possible to identify the changes in composition

311   due to fouling.

312   The main elements detected via EDX on cleaned membranes were C, O and F, and they result

313   evenly distributed over the surface due to the homogeneous nature of the ISE membrane (see

314   Appendix, Fig. A.7). Fluorine originates from the chemical composition of the PTFE protective

315   membrane layer. Other elements were detected in trace amounts on the cleaned membrane, which

316   were assumed deriving from the accumulation of dust over the membrane.

317   Since there is little F content in wastewater, fluorine is considered as the reference to compare the

318   elemental composition between the new and the fouled membrane. The fouled membrane results

319   (See Appendix. Table T.3; Fig. A.8) indicate a relative decrease in fluorine content (from 45

320   atomic % to 15 atomic %) while carbon and oxygen have increased dramatically: from 48 to 65

321   atomic % for C and from 5 to 18 atomic % for O. Other metal elements were detected in smaller

322   quantity in different portions of the fouled membrane's surface, such as Fe, Mn, P, N, Ca, Cl, S,

323   K, Mg, Na, S and Si, in descending order. Furthermore, the composition of the sensor fouling was

324   found to be comparable to the typical composition of fouling on filtration membranes found in

325   literature, in particular closely resembling the relative proportion between organic and inorganic

326   content.[41,45,46,47] The sensor's membrane fouling was primarily composed of organic pollutants,

327   while the inorganic matter contribution was minor. However, as reported by Wang et al. (2008)[42]

328   and Meng et al. (2007)[48], the inorganic elements such as Mg, Al, Fe, Ca, and Si have significant

329   effects on the formation of the gel layer. Such elements promote the bridging between deposited

330   biopolymers and inorganic compounds, while also enhancing the compactness of the fouling layer.

331   Therefore, although inorganic fouling may account for a relatively small amount of the overall

332   fouling, it does however influence the growth rate and structure of the organic fouling.

333   As expected, due to the practice of adding ferric chloride in the primary clarifiers, iron fouling is

334   consistently mapped by EDX over the entire surface of all the fouled membranes examined. In

335   detail, excluding the membrane composition and the organic fouling (C, O and F), iron was found

336   to be the most quantitatively abundant element of the inorganic fouling (26 atomic % of

337   Fe/inorganic fouling). The iron is hypothesized to mainly be present in the form of ferric oxides,

338   as commonly seen in literature.[38,49] Because Fe is detected in high content and is one of the trace

339   inorganic nutrients for bacteria that can enhance the development of biofouling,[19] we can infer it

340   could have also influenced the organic fouling build-up and future studies should address its role.

341   Therefore, iron plays a significant role in the general development of the irreversible fouling of

342   the sensor's membranes, as also was demonstrated in the studies of fouling in filtration

343   membranes.[48]

344   Most of the elements of the fouling, both organic and inorganic, such as C, O, F, Fe, Mn, and P,

345   are spread out evenly over the membrane surface (see Appendix, Fig. A.4). However, in some

346   spots of the fouled membranes some aggregates of K and Cl were observed. Since the mappings

347   of K and Cl agglomerates match perfectly, these are likely deposits of potassium chloride (KCl)

348   (see Appendix, Fig. A.9).

349   Figure 7 reports the details of EDX mappings on a crevasse (a) and on a damage of the membrane

350   surface (b). It can be noticed that the crevasse presents a local increase in fluorine concentration

351   (Fig. 7.a, in red), which could not be accounted by scaling/inorganic fouling considering the typical

352   low content of fluorine in wastewater. The high fluorine content on the membrane, instead,

353   originates from the PTFE coating, emerging from the thick layer of the fouling, showing the detail

354   of a fibrous-like stretched structure. Therefore, the EDX images further confirm the hypothesis of

355   the damaged PTFE, previously described when analysing the SEM mappings (Figure 6.b). A

356   further level of damage of the membrane was detected in other spots, observing fluorine and

357   chlorine mappings (Fig. 7.b, in yellow and red, respectively). In more than one spot (see Appendix,

358   Fig. A.10) similar patterns were noticed: i) large patches of high concentration of chlorine and ii)

359   uneven and scarce content of fluorine. However, this is in contrast with the typical elemental

360   pattern previously observed within the study, where fluorine is evenly distributed over the surface.

361   In terms of relative atomic proportion percent, the difference between the typical pattern and the

362   damage analysis is the following: the F content decreased from 15% to 9% and the Cl content

363   increased from 5% of the inorganic fouling to 23% of the inorganic fouling. The chlorine spots

364   could hardly derive from a precipitate due to the absence of the counter ion detected, as instead

365   shown in the Appendix Fig. A.9, and the irregular shape. Instead, it can be hypothesized that in

366   some regions of the membrane, the PTFE protective coating has been removed by abrasion, which

367   explains the observed decrease in fluorine content. The abrasion of the PTFE coating leaves the

368   underneath PVC $(C_2H_3Cl)_n$ layer of the membrane exposed, which helps to explain the increase in

369   irregular chlorine patches. Moreover, once the unprotected PVC membrane becomes exposed to

370   the external wastewater environment, it is easily and more rapidly degraded by bacterial activity,

371   thus further escalating the aging process of the electrodes. The damage areas of the PTFE coating

372   were attributed to the recurrent cleaning maintenance procedures performed during the six months

373   of operation. Thus, alternative cleaning methods should be considered in future studies, referring

374   also to the procedures deployed in filtration membrane cleaning, such as sonication and acid and

375   base cleaning.

376   **CONCLUSIONS**

377   In summary, the major impact of fouling on the sensor's performance is the increase of the

378   response time of the sensor to changes in ammonium concentrations. The effect of the fouling

379   development was found to promote a negative drift (-0.11 mg NH_4^+ $L^{-1}d^{-1}$), which is one order of

380   magnitude higher than the drift of a well-maintained sensor (-0.01 mg NH_4^+ $L^{-1}d^{-1}$), leading to an

381   underestimation of the ammonium content. This characterization of the sensor drift can provide a

382   quantitative reference for future studies on sensor fault detection and impact of sensor performance

383   on control systems.

384   The EDX analysis show that the inorganic fouling is mainly composed of Fe, P, Ca, Mn, S, K and

385   Cl, in decreasing order. The morphology and composition of the sensor's membrane fouling is

386   comparable to literature studies on filtration membrane fouling. Several fibrous cracks of the

387   protective PTFE coating were identified, as well as spots in the membrane where the PVC

388   membrane itself is exposed (patches of high content of chlorine), showing a further stage of

389   damage. The biomass composition has a high influence in the development and composition of

390   fouling. Therefore, the fouling study conducted can be considered as a reference limited to the site

391   condition (warm climates) and specific wastewater treatment application described. For a more

392   general conclusion and quantification of the effects of fouling over the ISE sensor performance

393   more studies should be conducted in different utilities, applications, and environmental conditions.

394   Also, to further supplement and support the data presented in the current paper, the development

395   of the fouling layer and its effects on the sensor behaviour over time should be further investigated

396   by impedance spectroscopy.

397

398
399

406

407

408　**REFERENCES**

409

410　1　M. A. Oneby, C. O. Bromley, J. H. Borchardt, D. S. Harrison, Ozone treatment of
411　　　secondary effluent at U.S. municipal wastewater treatment plants. *Ozone: Science &*
412　　　*Engineering*, 2010, **32**, 43-55.

413　2　D. Gerrity, B. Pecson, R. S. Trussel, R. R. Trussel, Potable reuse treatment trains
414　　　throughout the world. *Journal of Water Supply: Research & Technology*, 2013, **62**(6), 321-
415　　　328.

416　3　Metcalf & Eddy, Inc. Water Reuse: Issues, Technologies, and Applications (by Takashi
417　　　Asano et al. – 1st ed.), ISBN 0071459278, McGraw-Hill, New York, NY. 2007.

418　4　L. Rieger, I. Takács, H. Siegrist, Improving Nutrient Removal While Reducing Energy Use
419　　　at Three Swiss WWTPs Using Advanced Control. *Water Environ. Res.,* 2012a, **84** (2),
420　　　171–189.

421　5　L. Rieger, R. M. Jones, P. L. Dold, C. B. Bott, Ammonia-based feedforward and feedback
422　　　aeration control in activated sludge processes. *Water Environ. Res.*, 2014, **86** (1), 63-73.

423　6　P. Regmi, M. W. Miller, B. Holgate, R. Bunce, H. Park, K. Chandran, B. Wett, S. Murthy,
424　　　C. B. Bott, Control of aeration, aerobic SRT and COD input for mainstream
425　　　nitritation/denitrification. *Water Research*, 2014, **57**, 162-171.

426　7　S. B. Lewis & R. P. Buck, Optimizing Permselectivity for Neutral Carrier Membrane
427　　　Electrodes, *Analytical Letters*,1976, **9**(5), 439-449.

428   8   X. Zhang, F. Shi, J. Niu, Y. Jiang, Z. Wang, Superhydrophobic surfaces: from structural
429   control to functional application, *Journal of Materials Chemistry*, 2008, **18**, 621-633.

430   9   C-H. Xue, S-T. Jia, J. Zhang, J-Z. Ma, Large-area fabrication of superhydrophobic surfaces
431   for practical applications: an overview, *Science and Technology of Advanced Materials*,
432   2010, **11**, 033002.

433   10   K.S. Adu-Manu, C. Tapparello, W. Heinzelman, F. A. Katsriku, J.-D. Abdulai, Water
434   quality monitoring using wireless sensor networks: current trends and future research
435   directions, *ACM Transaction on Sensor Networks*, 2017, **13**, 1-41.

436   11   D. Ghernaout, M. Aichouni, A. Alghamdi, Applying big data in water treatment industry:
437   A new era of advance, *Int. Journal of Advanced and Applied Sciences*, 2018, **5**(3), 89-97.

438   12   M. Y. Schneider, J. P. Carbajal, V. Furrer, B. Sterkele, M. Maurer, K. Villez, Beyond signal
439   quality: the value of unmaintained pH, dissolved oxygen, and oxidation-reduction potential
440   sensors for remote performance monitoring of onsite sequencing batch reactors. *Water*
441   *Research*, 2019, **16**, 639–51.

442   13   M. Fettweis, R. Riethmuller, R. Verney, M. Becker, J. Backers et al., Uncertainties
443   associated with in-situ high-frequency long-term observations of suspended particulate
444   matter concentration using optical and acoustic sensors, *Progress in Oceanography*, 2019,
445   **178**, 102162.

446   14   T. Yang, H. Xiong, F. Liu, Q. Yang, B. Xu, C. Zhan, Effect of UV/TiO_2 pretreatment on
447   fouling alleviation and mechanisms of fouling development in a cross-flow filtration
448   process using ceramic UF membrane, *Chemical Engineering Journal*, 2019, **358**, 1583-
449   1593.

450   15   W. Yu, N. J. D. Graham, G. D. Fowler, Coagulation and oxidation for controlling
451   ultrafiltration membrane fouling in drinking water treatment: Application of ozone at low
452   dose in submerged membrane tank, *Water Research*, 2016, **95**, 1-10.

453   16   M. Aslam, A. Charfi, G. Lesage, M. Heran, J. Kim, Membrane bioreactors for wastewater
454   treatment: A review of mechanical cleaning by scouring agents to control membrane
455   fouling, *Chemical Engineering Journal*, 2017, **307**, 897-913.

456   17   W. Guo, H-H. Ngo, J. Li, A mini-review on membrane fouling. *Bioresource Technology*.
457   2012, **122**, 27-34.

458   18   X. M. Wang, T. D. Waite, Iron speciation and iron species transformation in activated
459   sludge membrane bioreactors. *Water Research*, 2010, **44**(11), 3511–3521.

460   19   M. Rebosura Jr., S. Salehin, I. Pikaar, X. Sun, J. Keller, K. Sharma, Z. Yuan, A
461   comprehensive laboratory assessment of the effects of sewer-dosed iron salts on
462   wastewater treatment processes, *Water Research*, 2018, **146**, 109-117.

463   20   M. Racar, D. Dolar, A. Spehar, A. Kras, K. Kosutic, Optimization of coagulation with
464   ferric chloride as a pretreatment for fouling reduction using nanofiltration of rendering
465   plant secondary effluent, *Chemosphere*, 2017, **181**, 485-491.

466   21   J. Wan, J. Gu, Q. Zhao, Y. Liu, COD capture: a feasible option towards energy self-
467   sufficient domestic wastewater treatment, Sci Rep, 2016, 6, 25054.

468   22   M. Mahdavi, M. M. Amin, Y. Hajizadeh, H. Farrokhzadeh, A. Ebrahimi, Removal of
469   different NOM fractions from spent filter backwash water by polyaluminum ferric chloride
470   and ferric chloride, Arab. J. Sci. Eng., 2017, 42, 1497-1504.

471   23   X. Li, Y. Liu, F. Liu, A. Liu, Q. Feng, Comparison of ferric chloride and aluminum sulfate
472   on phosphorous removal and membrane fouling in MBR treating BAF effluent of
473   municipal wastewater, *Journal of Water Reuse and Desalination*, 2017, **7**(4), 442-448.

474   24   A. H. Caravelli, E. M. Contreras, N. E. Zaritzky, Phosphorous removal in batch systems
475   using ferric chloride in the presence of activated sludges. *Journal of Hazardous Materials*,
476   2010, **177**(1–3), 199–208.

477   25   D. Rosso, and A. Al-Omari, *Carbon Capture and Management Strategies for Energy
478   Harvest from Wastewater*, Project U3R14/4879 Report, The Water Research Foundation,
479   Alexandria, VA. 2019.

480   26   ISO 15839. Water quality – On-line sensors/ Analysing equipment for water –
481   Specifications and performance tests, ISO 15839, ISO, Geneva, Switzerland. 2003.

482   27   L. Rieger, J. Alex, S. Winkler, M. Boehler, M. Thomann, H. Siegrist, Progress in sensor
483   technology - progress in process control? Part I: Sensor property investigation and
484   classification. *Water Science and Technology*, 2003, 47(2), 103 – 112.

485   28   W. E. Morf, E. Lindner, W. Simon, Theoretical treatment of the dynamic response of ion-
486   selective membrane electrodes, *Anal. Chem*. 1975, 47(9), 1596-1601.

487   29   C. G. Frankær, K. J. Hussain, M. Rosenberg, A. Jensen, B. W. Laursen, T. J. Sørensen,
488   Investigating the time response of an optical pH sensor based on a polysiloxane-

489   polyethylene glycol composite material impregnated with pH-responsive triangulenium
490   dye, *ACS Sens*. 2019, **4**, 8381-8389.

491 30 F. Cecconi, S. Reifsnyder, Y. Ito. M. Jimenez, R. Sobhani, D. Rosso, ISE-ammonium
492   sensors in WRRFs: field assessment of their influencing factors. *Environmental Science:*
493   *Water Research & Technology*, 2019, **5**(4), 737-746.

494 31 K. N. Mikhelson, AC-Impedance studies of ion transfer across ionophore-based ion-
495   selective membranes. *Chem. Anal*. 2006, **51**, 853-867.

496 32 E. L. Anderson and P. Buhlmann, Electrochemical Impedance Spectroscopy of Ion-
497   Selective Membranes: Artifacts in Two-, Three-, and Four-Electrode Measurements, *Anal.*
498   *Chem.* 2016, **88**, 9738-9745.

499 33 R. D. Armstrong, A. K. Covington, G. P. Evans, Mechanistic studies of the valinomycin-
500   based potassium-selective electrode using AC impedance methods, *Electroanal. Chem*.
501   1983, **159**, 33-40.

502 34 A. Radu, S. Anastasova-Ivanova, B. Paczosa-Bator, M. Danielewski, J. Bobacka, A.
503   Lewenstam, D. Diamond, Diagnostic of functionality of polymer membrane-based ion
504   selective electrodes by impedance spectroscopy. *Anal. Methods*, 2010, **2**, 1490-1498.

505 35 K. Ohmura, C. M. Thurlimann, M. Kipf, J. P. Carbajal, K. Villez, Characterizing long-term
506   wear and tear of ion-selective pH sensors. *Water Science & Technology,* 2018, **80**(3), 541-
507   550.

508 36 S. Papias, M. Masson, S. Pelletant, S. Prost-Boucle, C. Boutin, In situ continuous
509   monitoring of nitrogen with ion-selective electrodes in a constructed wetland receiving
510   treated wastewater: an operating protocol to obtain reliable data, *Water Science &*
511   *Technology*, 2018, **77**(4) 1706-1713.

512 37 C. Kazadi Mbamba, E. Lindblom, X. Flores-Alsina, S. Tait, S. Anderson, R. Saagi, D. J.
513   Batstone, K. V. Gernaey, U. Jeppsson, Plant-wide model-based analysis of iron dosage
514   strategies for chemical phosphorous removal in wastewater treatment systems, *Water*
515   *Research*, 2019, **155**, 12-25.

516 38 X. M. Wang, T. D. Waite, Iron speciation and iron species transformation in activated
517   sludge membrane bioreactors. *Water Research*, 2010, **44**(11), 3511–3521.

518 39 S. Jiang, Y. Li, B. P. Ladewig, A review of reverse osmosis membrane fouling and control
519   strategies. *Science of the Total Environment*, 2018, ***595***(October 2017), 567–583.

520 40 Y. An, Z. Wang, Z. Wu, D. Yang, Q. Zhou, Characterization of membrane foulants in an
521   anaerobic non-woven fabric membrane bioreactor for municipal wastewater treatment,
522   *Chemical Engineering Journal*, 2009, **155**, 709-715.

523 41 D. Al-Halbouni, J. Traber, S. Lyko, T. Wintgens, T. Melin, D. Tacke, A. Janot, W. Dott, J.
524   Hollender, Correlation of EPS content in activated sludge at different sludge retention
525   times with membrane fouling phenomena. *Water Res*. 2008, **42**, 1475–1488.

526 42 Z. Wang, Z. Wu, X. Yin, L. Tian, Membrane fouling in a submerged membrane bioreactor
527   (MBR) under sub-critical flux operation: Membrane foulant and gel layer characterization.
528   *Journal of Membrane Science*, 2008, **325**, 238-244.

529 43 G. Liu, C. Gao, X. Li, C. Guo, Y. Chen, J. Lv, Preparation and properties of porous
530   polytetrafluoroethylene hollow fiber membrane through mechanical operations. *J. Appl.*
531   *Polym. Sci.* 2015, **132**(43), 1–10.

532 44 K. Li, Y. Zhang, L. Xu, F. Zeng, D. Hou, J. Wang, Optimizing stretching conditions in
533   fabrication of PTFE hollow fiber membrane for performance improvement in membrane
534   distillation Optimizing stretching conditions in fabrication of PTFE hollow fiber membrane
535   for performance improvement in membrane distillation. *Journal of Membrane Science*,
536   2017, **550**(December), 126–135.

537 45 B. Zhang, B. Sun, M. Jin, T. Gong, Z. Gao, Extraction and analysis of extracellular
538   polymeric substances in membrane fouling in submerged MBR. *Desalination*, 2008,
539   **227**(1-3), 286-294.

540 46 Y. An, Z. Wang, Z. Wu, D. Yang, Q. Zhou, Characterization of membrane foulants in an
541   anaerobic non-woven fabric membrane bioreactor for municipal wastewater treatment.
542   *Chem. Eng. Journal*, 2009, **155**, 709–715.

543 47 P. Xu, C. Bellona, J. E. Drewes, Fouling of nanofiltration and reverse osmosis membranes
544   during municipal wastewater reclamation: Membrane autopsy results from pilot-scale
545   investigations. *Journal of Membrane Science*, 2010, **353**(1–2), 111–121.

546 48 F. G. Meng, H. M. Zhang, F. L. Yang, L. F. Liu, Characterization of cake layer in
547   submerged membrane bioreactor. *Environ. Sci. Technol.* 2007, **41**, 4065-4070.

548 49 Z. Zhang, M. W. Bligh, Y. Wang, G. L. Leslie, H. Bustamante, T. D. Waite, Cleaning
549   strategies for iron-fouled membranes from submerged membrane bioreactor treatment of
550   wastewaters. *Journal of Membrane Science*, 2015, **475**, 9–21.
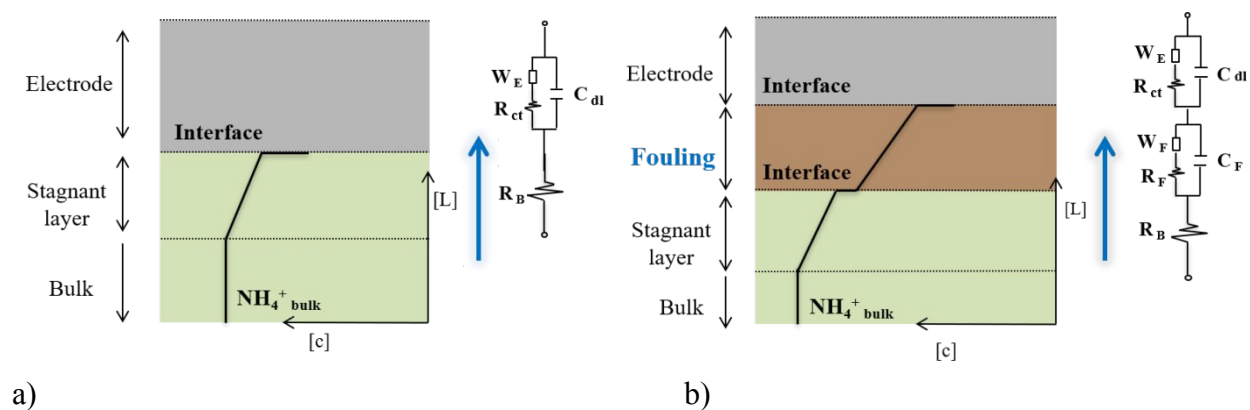
Figure 1. Illustration of the transport phenomena of the ammonium ions from the bulk of the wastewater to the sensor's membrane interface in cleaned (a) and in fouled conditions (b). (a) The overall transport process of ammonium in a cleaned membrane can be described by four equivalent circuit elements: R_B (bulk resistance), C_{dl} (double layer capacitance), R_{ct} (charge transfer resistance), and W_E (Warburg impedance). (b) In the presence of fouling the transport process presents an additional diffusional resistance in series between the stagnant layer and the electrode, described by a Warburg impedance W_F in series with a fouling layer resistance, R_F.

$k_{rise} = 0.10 \text{ s}^{-1}$

$k_{fall} = 0.12 \text{ s}^{-1}$

$R^2 = 0.96$

$k(t) = 0.95 \qquad \text{for } 0 < t < 1$

$k(t) = 0.95 * e^{-0.26t} \quad \text{for } t > 1$

$R^2 = 0.97$

a)   b)
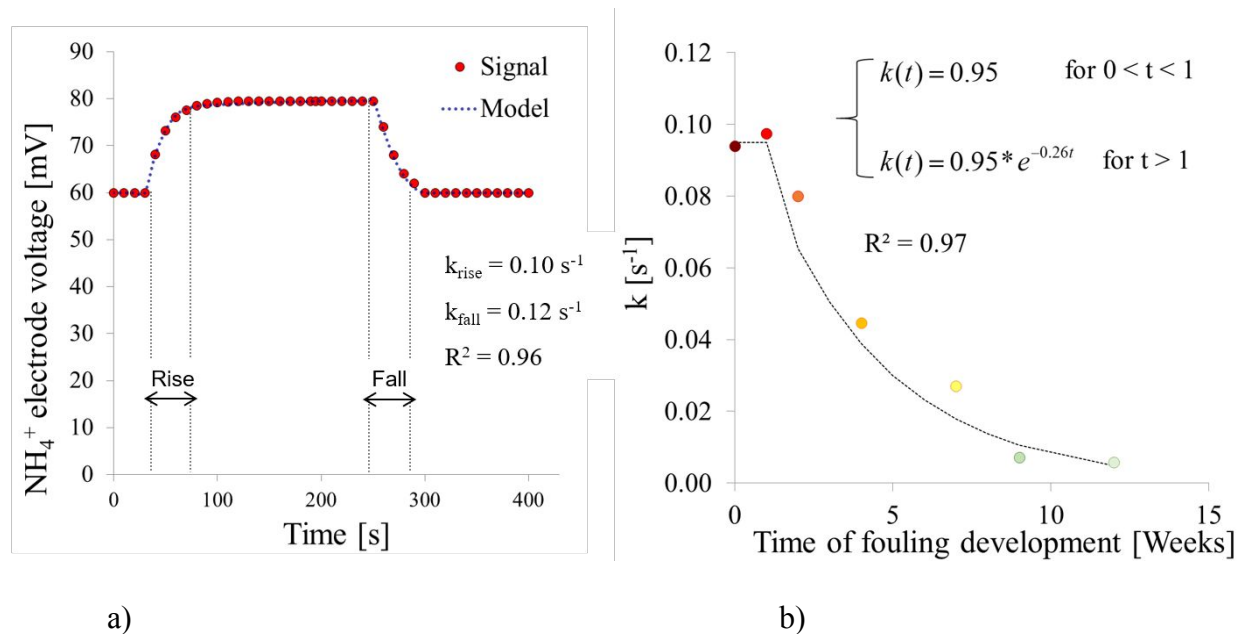
Figure 2.(a) Comparison between the sensor signal during a step-change experiment (in red) and the diffusion model (in blue), for cleaned conditions. (b) Volumetric mass transfer coefficient, k, as a function of the time of fouling development. The average measured volumetric mass transfer coefficient between rise and fall time is reported for each experiment conducted (circles). In detail, the results of the experiment in cleaned conditions (2.a) are represented by the red circle. The black dashed line represents the exponential model. Model equation and coefficient of determination, R^2, are reported in the graph.
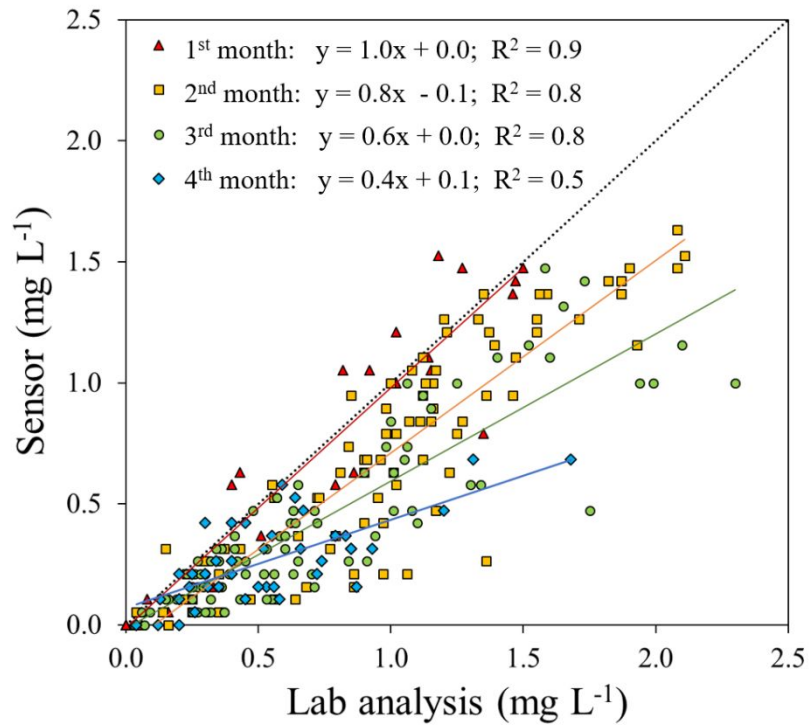
Figure 3. Comparison between sensor reading and lab analysis for 4 months of operation of the sensor. The dataset is divided into months, from the first month after the calibration of the sensor (red triangles) till the fourth month (blue diamonds). The linear trends of each month are shown, which equation and coefficient of determination, R^2, are reported in the graph.
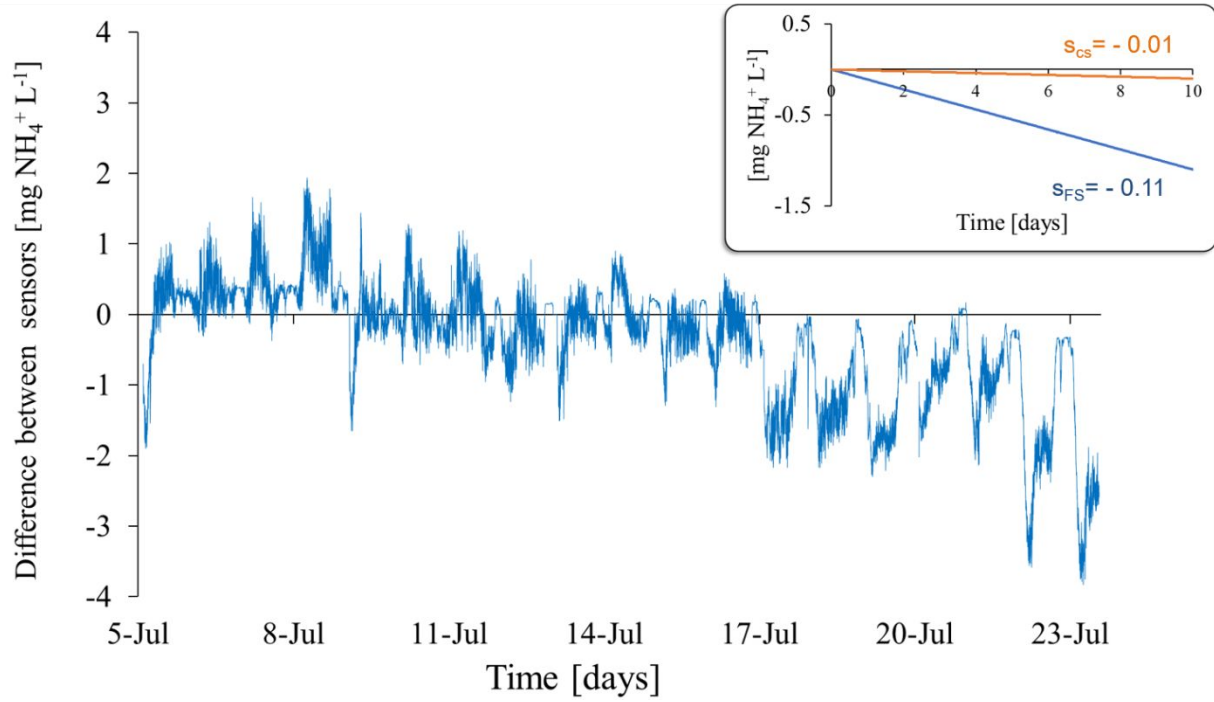
1

2   **Figure 4.** Difference between the cleaned and the fouled sensor signal, reported in blue with a 2-minute frequency.

3   s_{CS} = drift slope of the cleaned sensor in time (orange). s_{FS} = drift slope of fouled sensor in time (blue).

4

a)   b)
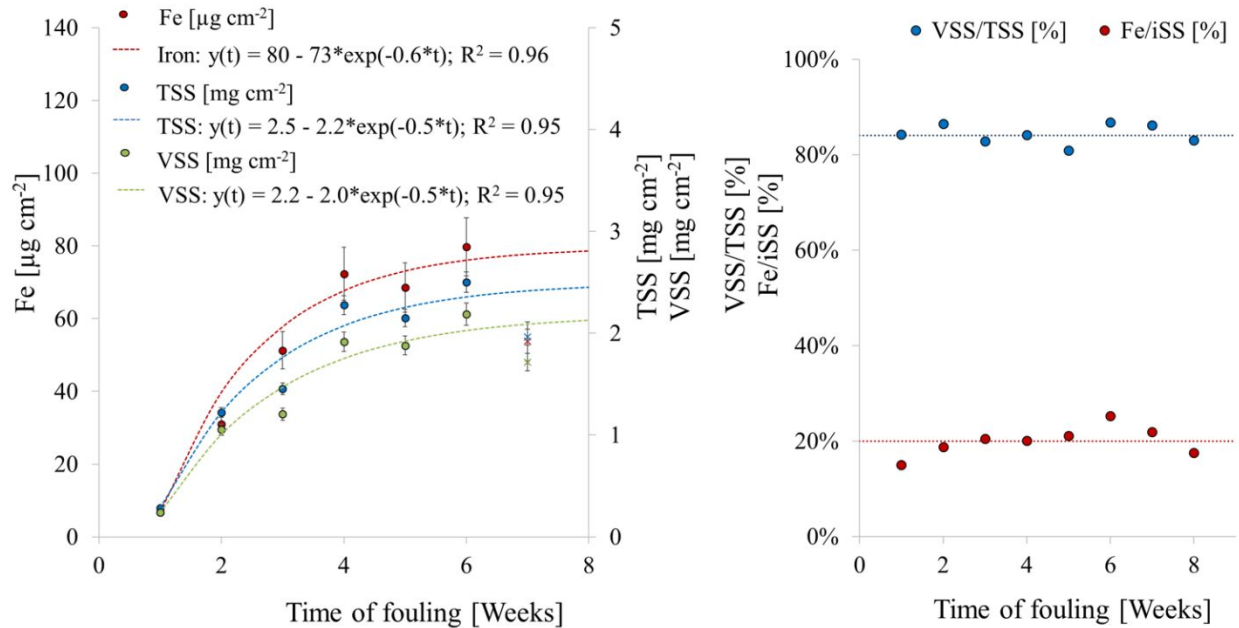
Figure 5. a) Trend of TSS, VSS and iron of the fouling layer, per unit of area, over time. The samples were collected from the membrane's surface electrodes of the rack. In blue are reported the TSS, in green the VSS and in red the iron content of fouling. The dashed lines represent the exponential model, with relative equation and coefficient of determination. The X markers show a foaming event of the treatment plant, and therefore are considered outliers. b) Trend of VSS/TSS (blue) and Fe/iSS (red) over the time of fouling, the dashed lines report the average value.
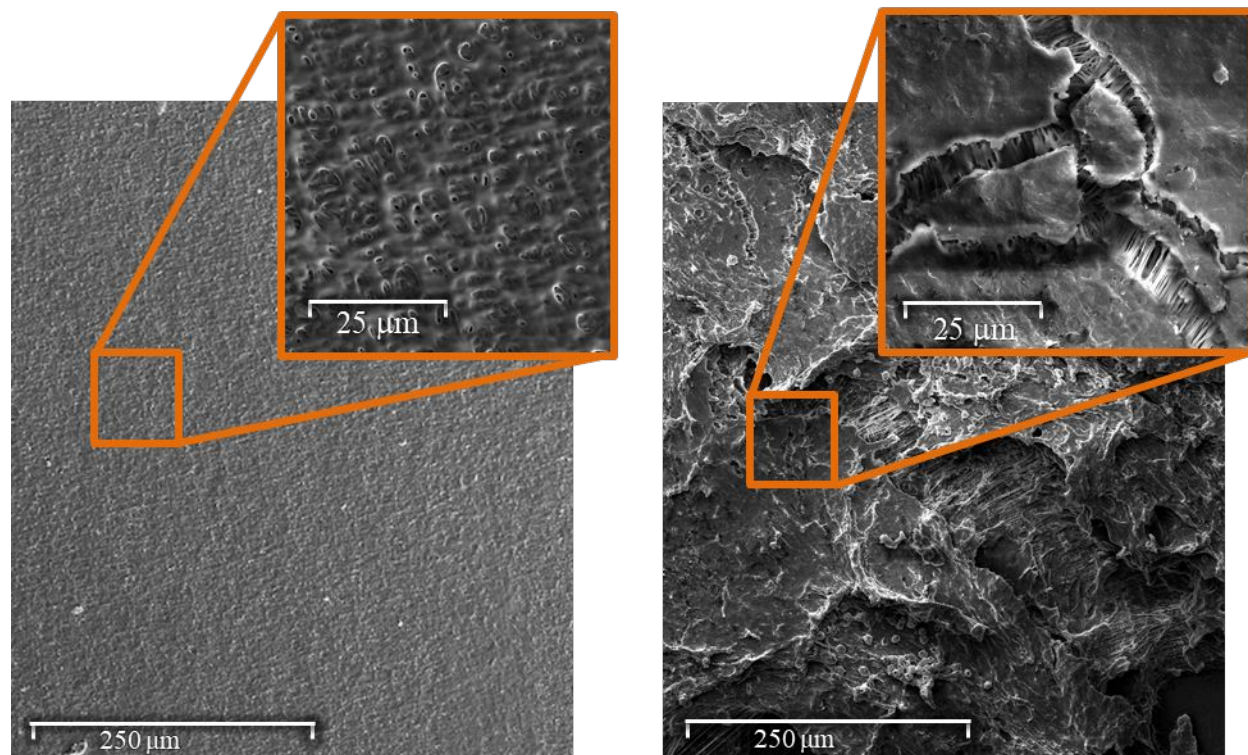
1

2　　a)　　　　　　　　　　　　　　　　　　b)

3　**Figure 6**. SEM images of the cleaned membrane (left) and fouled (right).

4

a)

b)
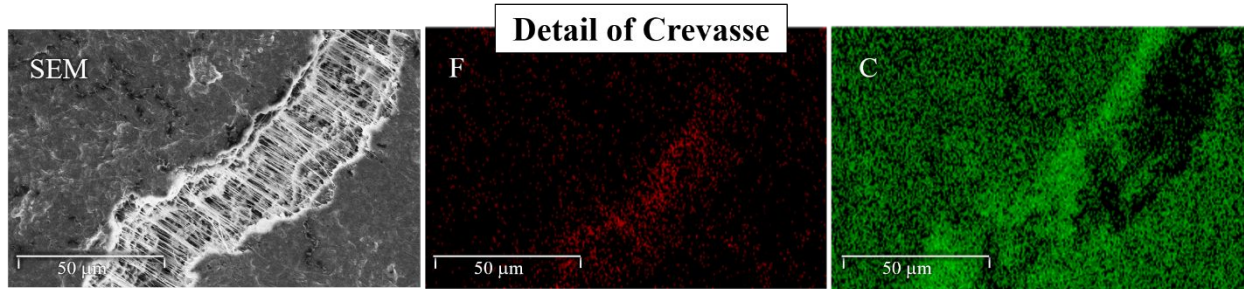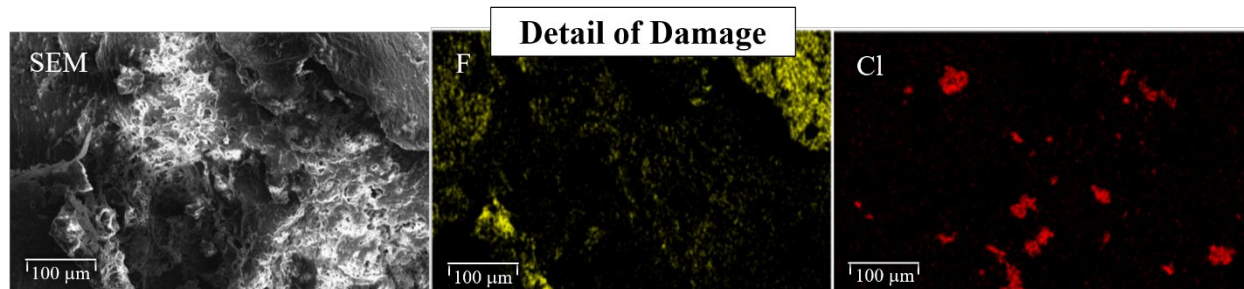
Figure 7. SEM and EDX elemental mappings of a fouled membrane are highlighted in different colours. (a) Detail of higher content of fluorine (red) and carbon (green) in the fouling layer over the crevasse, revealing the Teflon membrane $(C_2F_4)_n$ below. (b) Detail of damage images of fluorine (yellow) and chlorine (red) detected on a different spot of the fouled membrane.

Functional behaviour and microscopic analysis of ammonium sensors subject to fouling in activated sludge processes

Francesca Cecconi, Samuel Reifsnyder, Reza Sobhani, Albert Cisquella-Serra, Marc Madou, Diego Rosso
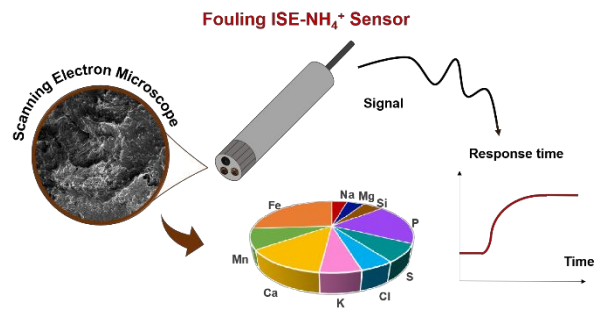
ISE-ammonium sensors subject to fouling display an increase in response time and an inexorable degradation of the measurement accuracy. Fouling morphology and composition were also studied by EDX analysis.